Ground-state structures and properties of $L1_0$ $Mn_{1-X}AlPt_X$ and $MnAl_{1-X}Pt_X$ alloys: a cluster expansion approach

Thabang Mokwena[1*], *Ramogohlo* Diale[2], *Phuti* Ngoepe[1], and *Hasani* Chauke[1]

[1] Materials Modelling Centre, University of Limpopo, South Africa,
[2]Advanced Materials Division, MINTEK, South Africa

Abstract. Permanent magnets play a crucial role in the development of technologies such as wind turbines and electric cars. Amongst permanent magnet, Nd-Fe-B magnets dominates the market due to its high magnetic moment . However, permanent magnets requiring heavy rare earth are hard to find, and their prices fluctuate. MnAl-based alloys have the potential to close the performance gap of Nd-Fe-B magnets. The ground-state structures and properties of $L1_0$ $Mn_{1-X}AlPt_X$ and $MnAl_{1-X}Pt_X$ alloys were investigated using Cluster Expansion (CE) and density functional theory (DFT). The accuracy of the CE prediction was assessed against DFT data, showing reasonable cross-validation scores of 0.08 and 1.10 since CVS< 5 meV/ pos. suggesting good cluster expansion prediction. CE generated 19 new favourable phases for $L1_0$ $Mn_{1-X}AlPt_X$ and 22 for $MnAl_{1-X}Pt_X$. The ground state line predicted 4 most favourably phases with negative formation energies for both $Mn_{1-X}AlPt_X$ and $MnAl_{1-X}Pt_X$ alloys, suggesting thermodynamic stability. The most thermodynamically stable phases from the Mn-site was found to be $MnPt_3Al_4$ (Mn-site) and Mn_2PtAl (Al-site) with the lowest formation energy of -0.046 eV and -0.330 eV, respectively. It was determined that those meeting the tetragonal stability criteria also satisfied the orthorhombic stability criteria. These findings will positively impact the development of permanent magnets for electric vehicles.

1 Introduction

Permanent magnets (PM) form an important part of advanced technology in the production of devices such as transport devices and memory devices [1]. This is due to their unique property of maintaining a high magnetic flux density when there is no external magnetic field. Amongst permanent magnets, Nd-Fe-B, SmCo, and ferrites have been studied a lot and are useful due to their unique properties such as adhesive force, acquisition cost, geometric design diversity, mechanical resistance, and magnetic stability [2]. Magnets made of Nd are more readily available than magnets made of other materials. These magnets were introduced as a replacement for SmCo magnets due to the high cost of samarium cobalt. This switch was also driven by the superior properties of Nd-Fe-B, which has an energy product of 60

* Corresponding author: mokwenathabang21@gmail.com

© The Authors, published by EDP Sciences. This is an open access article distributed under the terms of the Creative Commons Attribution License 4.0 (https://creativecommons.org/licenses/by/4.0/).

MGOe, compared to 55 MGOe for SmCo [3]. Currently, the prices of permanent magnets containing heavy rare earths like Dy, Tb, and Sm fluctuate greatly. In the absence of more abundant alternative materials, it is predicted that these elements will become scarce in the upcoming decades. In this regard, the development of rare earth-free permanent magnets becomes increasingly important.

Recently, there has been a lot of interest in Mn-based intermetallic alloys because of their distinctive hard magnetic properties and low price [4]. Among those, the ferromagnetic $L1_0$-MnAl phase has drawn a lot of interest lately due to its elevated Curie temperatures and strong magnetic moments [5]. However, MnAl alloy faces several drawbacks, such as brittleness and limited thermodynamic stability. Researchers are currently exploring approaches to enhance MnAl alloy to achieve excellent thermodynamic stability and ductility. For instance, doping MnAl with carbon (C) appears promising for enhancing stability, at the expense of reducing the Curie temperature of τ-MnAl [6]. It is widely recognized that the metastable τ-phase in binary MnAl alloys quickly transition to the balance between γ2 and β-Mn phases. and that this transformation is irreversible. In another study, the magnetic qualities of Fe-doped MnAl were determined to explore the magnetic characteristics of $L1_0$-structured $Fe_xMn_{1-x}Al$ alloys using VASP code [7]. The study demonstrated that introducing Fe enhanced the magnetocrystalline anisotropy, this is associated with a rise in the density of states at the Fermi level for minority electrons.. In this paper, Cluster expansion and DFT were employed to determine ground-state structures and properties of ternary $L1_0$-$Mn_{1-X}AlPt_X$ and $MnAl_{1-X}Pt_X$ alloys [8].

2 Methodology

2.1 Cluster expansion

The ground-state structures of $L1_0$-$Mn_{1-X}AlPt_X$ and $MnAl_{1-X}Pt_X$ were studied using the UNCLE code [9] performed in MedeA environment. To understand the ground-state structure and phase stability of these alloys, total energy must be calculated for each possible configuration. The cluster expansion (CE) technique [10, 11] served to determine the configurational total energy of various alloys. For the various atomic configurations, the cluster expansion (CE) technique constructs an Ising-like Hamiltonian. UNCLE code [9] was used to automate most of the steps involved in constructing the CE Hamiltonian and calculating thermodynamic characteristics based on the CE method. UNCLE expands the cluster expansion by adding new clusters progressively till the necessary precision is obtained. This code may finish the CE fit if more than two items are present. Each iteration's initial training set comprised at least four structures, and the CE could have a maximum of four or more structures. The CE can proceed after a certain amount of iterations has been successfully achieved. This approach is repeated until the energy of every structure can be calculated utilizing the CE at various concentrations.

2.2 Density Functional Theory calculation

The density functional theory (DFT) performed in the Vienna ab initio simulation package (VASP) [12, 13] was employed to determine the first-principles total energy for a given atomic configuration of $L1_0$-$Mn_{1-X}AlPt_X$ and $MnAl_{1-X}Pt_X$. A projector augmented wave (PAW) [14] technique was employed to define the interaction between the core and valence electrons. For plane waves, an energy cut-off of 500 eV was used in the expansion of wave functions. The cell volume, form, and positions of the atoms were left to relax until the stress was low and the forces on any atom were less than 0.02 eV/É. This was done to get structural

full optimization. The Perdew-Burke-Ernzerhof (PBE) generalized gradient approximation (GGA) functional was used to explain the exchange-correlation energy. [15, 16]. A parameter sets an automatic k-point mesh generation for systems with 0.2 k-spacing when UNCLE code [9] is utilized as a script link to VASP. Only the spin-orbit coupling was considered in the force theorem computation.The ground-state structures' elastic constants were computed using a strain of 0.005.

3 Results and discussion

3.1 Ground state structures

Figure 1 illustrates the formation energies ΔE_f (σ) they were utilized to fit the cluster expansion Hamiltonians. Once the ground states for a variety of concentrations have been established, the convexity requirement determines which are stable at T=0 K; that is, if the phases at concentration x sits below any straight line joining other compounds at concentrations, it is stable. Figure 1 shows that $L1_0$-$MnAl_{1-X}Pt_X$ structures have negative ΔE_f (σ), while those surrounding the convex hull contribute to its miscibility. Structures that form vertices on the hull's lower boundary are stable structures. The generated ground state structures as shown by the ground state line are MnPt, Mn_4Pt_3Al, $(Mn2PtAl)_2$, and MnAl. The most stable structure is found to be $(Mn_2PtAl)_2$ (Cmmm) with the smallest formation energy as compared to other systems. Table 1 displays the projected number of structures together with their cross-validation score. The fully optimized ternary ground state diagram predicted 22 new compounds. The CVS was used to assess the predictive capability of the cluster expansion. The study's cluster expansion has a low CVS (<5) indicating good fitting accuracy. In this case, CVS is 1.10 meV/pos, this indicates good cluster expansion (CVS < 5 meV/pos).

Figure 2 illustrates the ground-state phases of the alloy compositions of $L1_0$ $Mn_{1-X}AlPt_X$. The ground-state structures, outlined in red, are regarded thermodynamically stable. The ground state line shows four stable structures based on the estimated formation energy. The circles indicate energy for certain configurations, as determined by DFT computations and CE predictions. The predicted structures were found to be thermodynamically stable due to negative formation energies. The CE estimated stable structures of various compositions and space groups.The predicted ground-state structures were found to be PtAl, $(MnPt_3Al_4)_2$, $(MnPt2Al_3)_2$, and MnAl with distinct space groups. Thus, the results showed that the $(MnPt_3Al_4)_2$ (Cmmm) is the most thermodynamically stable structure due to the smallest formation energy (ΔE_f = -0.02 meV/atom) as compared other structures. These results are reliable because excellent convergence was achieved with the cluster expansion (CE). Table 1 also shows the number of new compositions and the cross-validation score (CVS) for $L1_0$-$Mn_{1-X}AlPt_X$ .The cluster expansion predicted 19 new compounds of the $L1_0$-$Mn_{1-X}AlPt_X$ system. It is noted that CVS is 0.08 meV/pos., this is likewise suitable as recommended above, given CVS < 5 meV/pos implies good cluster expansion.

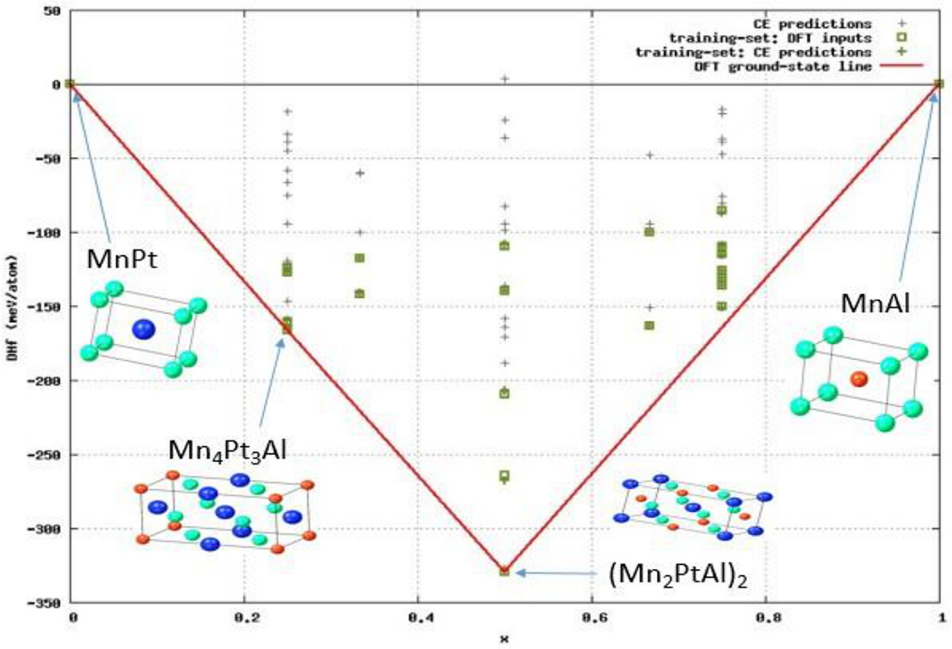

Fig. 1. Ground state line of the ternary $L1_0$-$MnAl_{1-X}Pt_X$ systems formation energy against Pt concentration.

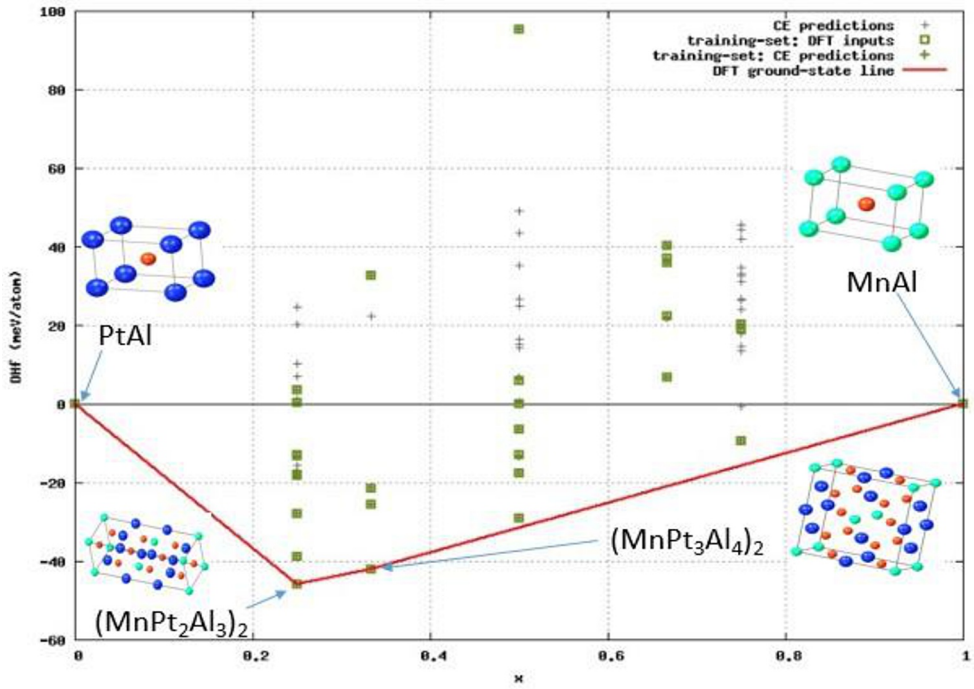

Fig. 2. Ground state line of the ternary of $L1_0$-$Mn_{1-X}AlPt_X$ systems formation energy against Pt concentration.

Table 1. Characteristics of the calculated cluster expansion of Mn-Al-Pt.

Characteristics	**$L1_0$-$Mn_{1-X}AlPt_X$**	**$L1_0$-$MnAl_{1-X}Pt_X$**
Number of new structures	19	22
Number of ground-state structures	4	4
Cross-validation scores (meV/pos.)	0.08	1.10

3.2 Optimized ground-state structures from cluster expansion

Table 2 presents the equilibrium lattice parameters and magnetic properties for the $L1_0$-$Mn_{1-X}AlPt_X$ and $MnAl_{1-X}Pt_X$ alloy compositions. This data is used to evaluate the effect of Pt doping on the $L1_0$ phases of the Mn and Al sublattices. The structures underwent complete geometry optimization, adjusting both the lattice constant and the form. The measured lattice parameters were compared to theoretical values to validate the binary model (Mn50Al50). The predicted lattice parameters for the binary $Mn_{50}Al_{50}$ are a=2.749 (2.753) and c=3.514 (3.500) [6], which are within 5% of the theoretical data (values in parentheses).

Table 2. The generated lattice parameters and magnetic moments of $L1_0$-$Mn_{1-X}AlPt_X$ and $MnAl_{1-X}Pt_X$.

Structures	**Space group**	**a(Å)**	**b(Å)**	**c(Å)**	**Magnetic moment ($\mu B/atom$)**
$L1_0$-$Mn_{1-X}AlPt_X$					
MnAl	(P4/mmm)	2.749	2.749	3.514	2.352
$(MnPt_3Al_4)_2$	(Cmmm)	4.035	3.517	2.010	0.156
$(MnPt_2Al_3)_2$	(Cmmm)	4.001	3.998	3.514	0.169
PtAl	(P4/mmm)	3.199	3.199	2.882	0.000
$L1_0$ $MnAl_{1-X}Pt_X$					
MnAl	(P4/mmm)	2.749	2.749	3.514	2.352
Mn_4Pt_3Al	(P4/mmm)	3.974	3.974	3.728	1.912
$(Mn_2PtAl)_2$	(I4/mmm)	3.812	3.812	3.915	0.862
MnPt	(P4/mmm)	2.944	2.944	3.484	4.415

The magnetic moment was assessed to evaluate the magnetic intensity of the ground state structures. Table 2 shows that magnetic moments drop as Pt increases. Given that PtAl has antiferromagnetic properties and zero magnetic moments, it is concluded that placing Pt on the Mn-site has no effect on ferromagnetic behavior.

The lattice parameters for the binary $L1_0$-MnAl are a = 2.749 Å (2.753 Å) and c = 3.514 Å (3.500 Å), which shows good agreement with the results (values in parentheses) to within 5% (c/a = 1.30) (1.30) [17]. Table 2 indicates that the addition of Pt to the Al-site generally results in a decrease in the magnetic moment of the $L1_0$-$MnAl_{1-X}Pt_X$ alloys, with the exception of MnPt. MnPt exhibits a higher magnetic moment (4.415) compared to the other ground-state structures. The results also reveal that $(Mn_2PtAl)_2$ displays weak ferromagnetic

behavior, with a magnetic moment close to zero. This suggests that Pt is ineffective in enhancing the magnetism of MnAl at both the Al and Mn sites.

3.3 Elastic properties

Assessing the elastic properties of materials is essential as it helps investigate the mechanical stability of a material based on its elastic constants (C_{ij}). The elastic constants are critical for determining material strength, as they indicate how crystals respond to macroscopic stresses. From the literature, evaluations have been conducted of various systems with different symmetries in the past, including cubic, tetragonal, orthorhombic, and monoclinic structures [18, 19]. There are six independent elastic constants (C_{11}, C_{12}, C_{13}, C_{33}, $C_{44,}$ and C_{66}.) for tetragonal crystal structures. The mechanical stability condition for tetragonal system as outlined [19] is given as follows:

$$C_{44} > 0,\ C_{66} > 0,\ C_{11} > |C_{12}|\ \text{, and}\ C_{11} + C_{12} - \frac{2C_{13}^2}{C_{33}} > 0. \quad (1)$$

There nine independent elastic constants (C_{11}, C_{12}, C_{13}, $C_{22,}$ $C_{23,}$ C_{33}, $C_{44,}$ C_{55}, and C_{66}.) for orthorhombic crystal structures and mechanical stability criteria are as follows [18]:

$$C_{11} > 0, C_{22} > 0, C_{33} > 0, C_{44} > 0, C_{55} > 0, C_{66} > 0,\ (C_{11} + C_{22} + 2C_{12}) > 0,\ (C_{11} + C_{33} - 2C_{13}) > 0,\ (C_{22} + C_{33} - 2C_{23}) > 0, (C_{11} + C_{22} + C_{33} + 2C_{12} + 2c_{13} + 2C_{23}) > 0 \quad (2)$$

The binary $L1_0$ MnAl alloy demonstrates mechanical stability attributed to its positive elastic shear modulus. Consequently, the introduction of a third element has been proposed to evaluate its impact on the elastic constants of the binary system. As presented in Table 3, the predicted Cij values for $L1_0$-$Mn_{1-X}AlPt_X$ do not meet the established stability criteria. The Cij values for ternary additions are lower than those observed in the binary MnAl structure, indicating that the doping element Al lacks the capacity to enhance the Cij of the $L1_0$ phase. In contrast, for L10-$MnAl_{1-X}Pt_X$ alloys, all predicted structures exhibit mechanical stability, satisfying the required stability conditions. Notably, MnAl displays the highest elastic constant values, suggesting that the structure achieves maximum stability at this composition, as demonstrated in Table 3.

Table 3. The elastic constants of the ground state structures.

Structure	**C_{11}**	**C_{12}**	**C_{13}**	**C_{22}**	**C_{23}**	**C_{33}**	**C_{44}**	**C_{55}**	**C_{66}**
$L1_0$-$Mn_{1-X}AlPt_X$									
MnAl	283.91	41.98	102.82			146.12	120.96		62.96
$(MnPt_3Al_4)_2$	239.70	133.40	107.80	196.89	141.54	239.77	79.78	89.87	79.93
$(MnPt_2Al_3)_2$	275.96	133.33	122.28	270.49	125.23	215.36	83.69	80.04	128.00
PtAl	175.85	176.59	203.62			151.24	77.63		75.98
$L1_0$-$MnAl_{1-X}$ Pt_X									
MnAl	283.91	41.98	102.82			146.12	120.96		62.96
Mn_4Pt_3Al	178.08	88.67	123.03			188.20	89.78		85.17
$(Mn_2PtAl)_2$	178.80	119.90	105.69			183.59	82.42		76.24
MnPt	251.28	88.57	147.79			228.95	97.92		72.63

Table 4 illustrates the calculated Pugh's (B/G) and Poisson's ratio of the predicted ground state structures of $L1_0$-$Mn_{1-X}AlPt_X$ and $MnAl_{1-X}$ Pt_X alloys. Pugh suggested Bulk-to-Shear (B/G) modulus ratios to evaluate the ductility/brittleness of the material [20]. A B/G ratio above 1.75 signifies that the material is ductile, while a ratio below 1.75 indicates brittleness.

MnAl is classified as brittle due to its Pugh ratio being less than 1.75, specifically 1.46. In contrast, $(MnPt_3Al_4)_2$ has a Pugh ratio of 2.311, which is above 1.75, indicating ductility. Similarly, $(MnPt_2Al_3)_2$ exhibits a Pugh ratio of 2.021, also above the critical value, signifying ductility. Moreover, PtAl, with a B/G value of 4.543, significantly exceeds 1.75, confirming its ductile nature. In the case of $MnAl_{1-X}Pt_X$ alloys, Mn_4Pt_3Al has a Pugh ratio of 2.015, exceeding the critical value of 1.75, indicating ductility. Additionally, the Pugh ratio of $(Mn_2PtAl)_2$ is 2.150, which is also above 1.75, signifying that the material is ductile. On the other hand, MnPt, with a Pugh ratio of 0.300, falls below the critical value, indicating brittleness.

The Poisson's ratio is also used to determine a material's ductility. If a material's Poisson ratio is less than 0.26, it is considered brittle; a positive Poisson ratio, on the other hand, implies ductile behaviour. The brittleness of MnAl is characterized by a Poisson ratio of 0.221, which falls below the critical value of 0.26, indicating its brittle nature. Conversely, $(MnPt_3Al_4)_2$ exhibits ductile behavior with a Poisson ratio of 0.311, surpassing the critical threshold. Similarly, $(MnPt_2Al_3)_2$ is identified as ductile, with a Poisson ratio of 0.287, exceeding the critical value of 0.26. PtAl demonstrates ductility, as evidenced by its Poisson ratio of 0.398, which is significantly higher than the critical threshold. In the $MnAl_{1-X}Pt_X$ system, Mn_4Pt_3Al shows ductility with a Poisson ratio of 0.287, above the crucial value of 0.26. Likewise, $(Mn_2PtAl)_2$ is classified as ductile due to its Poisson ratio of 0.300, which is above the critical limit. Furthermore, the Poisson ratio of 0.300 for MnPt, significantly above the critical value of 0.26, confirms its ductility.

Table 4. The Pugh and Poisson ratios of the ground state structures.

Structures	Pugh ratio	Poisson ratio
$L1_0$-$Mn_{1-X}AlPt_X$		
MnAl	1.459	0.221
$(MnPt_3Al_4)_2$	2.311	0.311
$(MnPt_2Al_3)_2$	2.021	0.287
PtAl	4.543	0.398
$L1_0$-$MnAl_{1-X}Pt_X$		
MnAl	1.459	0.221
Mn_4Pt_3Al	2.015	0.287
$(Mn_2PtAl)_2$	2.150	0.300
MnPt	2.168	0.300

4 Conclusion

The phase stability of the $L1_0$-$Mn_{1-X}AlPt_X$ and $MnAl_{1-X}Pt_X$ alloys was examined using DFT and Cluster expansion. The cluster expansion approach was successfully employed to create twenty-two new structures on $L1_0$-$MnAl_{1-X}Pt_X$ and nineteen new structures on $L1_0$-$Mn_{1-X}AlPt_X$. The majority of the structure formation energies in the data were negative, indicating the phase stability of both $L1_0$-$Mn_{1-X}AlPt_X$ and $MnAl_{1-X}Pt_X$ alloys. For $L1_0$-$Mn_{1-X}AlPt_X$ and $MnAl_{1-X}Pt_X$, respectively, $(MnPt_3Al_4)_2$ and $(MnPt_3Al_4)_2$ are shown to be the most thermodynamically stable structures with the smallest energy. Additionally, PtAl was shown to have zero magnetic moment antiferromagnetic behavior. This suggests that the introduction of Pt on either site of MnAl does not significantly enhance its magnetic properties. The elastic constants and ratios were used to check were the structures satisfy different stability criteria and whether they are ductile or brittle. As a result, this study has

shown that CE can be applied to gain a deeper understanding of the phase stability of developing magnets.

The Materials Modelling Centre, the University of Limpopo, and the Centre for High-Performance Computing (CHPC) in Cape Town provided computer resources for the computations. The Department of Science and Innovation (DSI)'s Advanced Materials Initiative (AMI) through Mintek provided funding assistance, which the authors appreciate. We are grateful for the Department of Science and Innovation's support of the South African Research Chair Initiative.

References

1. A. J. J. Koch, P. Hokkeling, M.G. vd Steeg, K.J. De Vos, Appl. Phys. **31**, S75-S77 (1960).
2. J. Coey, Phys.: Condens. Matter **26**, 064211 (2014).
3. L. Zheng, L. Yue, L. Su, M. Zhu, Y. Fang, L. Zhao, L. Wu, W. Li, Miner. Met. Mater. Soc., (2024).
4. J. M. D. Coey, Scripta Mater. **67**, 524-529 (2012).
5. R. F. C. Farrow, R. F. Marks, S. Gider, A. C. Marley, S. S. P. Parkin, D. Mauri, Appl. Phys. **81**, 4986-4988 (1997).
6. I. D. Sebe, M. E. Sithole, R. Modiba, (2022).
7. P. Manchanda, A. Kashyap, J. E. Shield, L. H. Lewis, R. Skomski,, Magn. Magn. Mater. **365**, 88-92 (2014).
8. S. Zhao, Y. Wu, C. Zhang, J. Wang, Z. Fu, R. Zhang, C. Jiang, Alloys Compd. **755**, 257-264 (2018).
9. D. Lerch, O. Wieckhorst, G.L.W. Hart, R.W. Forcade, S. Müller, Modell. Simul. Mater. Sci. Eng. **17**, 055003 (2009).
10. J. M. Sanchez, F. Ducastelle, D. Gratias, Physica A **128**, 334-350 (1984).
11. A. van de Walle, M. Asta, G. Ceder, CALPHAD **26**, 539-553 (2002).
12. G. Kresse, J. Hafner, Phys. Rev. B **47**, 58-561 (1993).
13. G. Kresse, J. Furthmüller, Phys. Rev. B **54**, 11169-11186 (1996).
14. P. E. Blöchl, Phys. Rev. B **50**, 17953-17979 (1994).
15. J. P. Perdew, K. Burke, M. Ernzerhof, Phys. Rev. Lett. **77**, 3865-3868 (1996).
16. W. Kohn, L.J. Sham, Phys. Rev. **140**, 1133-1138 (1965).
17. N. Singh, V. Mudgil, K. Anand, A. K. Srivastava, R. K. Kotnala, and A. Dhar, Alloys Compd. **633**, 401-407 (2015).
18. R. Mahlangu, M.J. Phasha, H.R. Chauke, P.E. Ngoepe, Intermetallics **33**, 27-32 (2013).
19. N. L. Lethole, H. R. Chauke, P. E. Ngoepe, Comput. Theor. Chem. **1155**, 67-74 (2019).
20. K. A. Matori, M.H.M. Zaid, H. A. A. Sidek, M. K. Halimah, Z. A. Wahab, M.G.M. Sabri, Int. J. Phys. Sci. **5**, 2212-2216 (2010)